

# A Kinetic Study of Electron-Wall Collisions in a Hall Thruster<sup>\*†</sup>

Nathan B. Meezan and Mark A. Cappelli  
Stanford University  
Department of Mechanical Engineering  
Stanford, CA 94305-3032

IEPC-01-51

**The role of electron-wall collisions in Hall thruster operation is studied through simulation of the electron energy distribution function (EEDF) inside the thruster channel. The electron Boltzmann equation is solved using the “local-field” approximation, using experimental results as input data. The equation takes into account inelastic losses due to ionizing collisions and wall-collisions, as well as secondary electrons from ionization and from wall-collisions. Electron balances are used to calculate the sheath potential at the insulator walls. Results show an EEDF cut off at high energy due to electron loss to the walls. The calculated EEDFs agree well with experimental electron temperature data when an experimentally-determined effective collision frequency is used for electron momentum transport. Predicted values for the wall-sheath potential agree with results of a Maxwellian flux-balance, but only when secondary electron generation is neglected. The electron wall-loss and wall-return frequencies are extremely low compared to those predicted by a Maxwellian of equal average energy, a difference due solely to the shape of the simulated EEDF. The very low wall-collision frequency suggests that for this particular laboratory Hall thruster, secondary electrons do not contribute to cross-field transport.**

## Introduction

Hall discharges (Hall thrusters) are presently under development for use in space propulsion applications. The electrons in Hall discharges exhibit anomalous cross-field transport: the conductivity is higher than that predicted by the simplest classical equations. Electron transport in the Hall thruster is believed to be enhanced by fluctuations in the electric field and plasma density [1]; however, collisions with the thruster channel walls also play an important role in discharge operation. In addition to impacting the kinetics of the Hall discharge plasma by shaping the electron energy distribution function (EEDF), the electron-wall interaction in the channel can also contribute to electron transport via “near-wall conductivity.”

Understanding the EEDF inside the discharge channel is critical to successful thruster modeling, as the EEDF links the electron-wall interaction and the

ionization process to the electric and magnetic fields in the plasma. In previous studies, analytical, experimental, and numerical approaches to finding the EEDF have been used to gain insight into thruster physics in general and the electron-wall interaction in particular. Unfortunately, the EEDF is a difficult problem to tackle. Experimental measurements of the EEDF rely almost entirely on Langmuir probe theories of dubious value in magnetized plasmas. Simulations of the EEDF can provide physical insight, but obtaining quantitative results requires simulation of the entire plasma. In addition, exact physical mechanisms for the electron-wall interaction are not well known, so phenomenological models are often needed.

In this study, we use an alternative approach: we use experimentally-determined plasma properties and a simplified Boltzmann equation to calculate the EEDF. The model also uses electron balances in the channel to calculate the wall-sheath potential in a self-

---

\* Presented as Paper IEPC-01-051 at the 27<sup>th</sup> International Electric Propulsion Conference, Pasadena, CA, 15-19 October, 2001.

† Copyright 2001 by Stanford University. Published by the Electric Rocket Propulsion Society with permission.

consistent way, rather than invoking the no-current condition at the wall. This method of in-depth data analysis is instructive rather than predictive, providing insight into Hall thruster physics without full simulation of the plasma. We use this Boltzmann equation model to compare and discuss different ideas about anomalous conductivity, mechanisms of EEDF formation, and electron-wall interaction.

## Background

The idea of near-wall conductivity in Hall thrusters was developed primarily by Morozov. In a series of papers in 1984 [2-4], Morozov developed a mechanism for near-wall conductivity for the case of no gas-phase collisions. The basic idea is elucidated in [3]. There are two different classes of electrons in the plasma. Low energy electrons scatter specularly and elastically off the wall-sheath, and therefore must rely on gas-phase collisions or wave-interactions to drift to the anode. High energy electrons that can penetrate the sheath scatter diffusely and elastically off the wall, gaining an additional mechanism for cross-field transport. This results in an EEDF with separate populations of “slow” electrons and “fast” electrons because there is no mechanism for thermalization. Fast electrons, able to cross the magnetic field lines with no price in energy, can reach very high energies (several times the ionization threshold) by the time they reach the anode. Some experimental measurements of the EEDF in an Hall thruster by Bugrova [5,6] reveal a “double-hump” distribution near the anode, presumably due to separate populations of fast and slow electrons.

This idea of near-wall conductivity was further explored by Degond *et al.* in 1998 [7]. For the case of no gas-phase collisions, Degond solves the electron Boltzmann equation using a Hilbert expansion method and compares the results to a Monte Carlo simulation. Both models reproduce the “double-hump” EEDF, with the energy of the second hump increasing towards the anode. Later versions of these models, expanded to include elastic and inelastic gas-phase collisions, produced similar results [8]. The two-population distribution remained, although the height of the high-energy peak was slightly diminished, presumably due to increased thermalization. The phenomenological model for the electron-wall interaction used in these studies describes several

classes of scattered electrons and will be explained further in a later section.

Although the idea of separate slow and fast electron populations is consistent with some experimental measurements of the EEDF, it is worth noting that analyses based on other mechanisms can reproduce the experimentally-measured “double hump” distribution. A study by Fedotov *et al.* used a different model for the EEDF to explain the multiple humps in a measured EEDF [9]. In this analytical model, the collisionless integrals of motion for the electrons are substituted into a Maxwellian electron velocity distribution function (EVDF). The two humps in the resultant EEDF are due not to distinct populations of electrons, but to the fast  $\mathbf{E} \times \mathbf{B}$  drift of the electrons.

## Theory

The derivation of the simplified Boltzmann equation used in this study was presented in a previous paper [10] but is included here for completeness. The model for electron-wall interaction has been slightly changed. The complete EEDF model is summarized at the end of the section.

### Approximations and simplifications

The steady-state Boltzmann equation for the electrons can be written as

$$\mathbf{c} \nabla_x f - \frac{e}{m} (\mathbf{E} + \mathbf{c} \times \mathbf{B}) \nabla_c f = \left( \frac{\delta f}{\delta t} \right)_{coll.}, \quad (1)$$

where  $f$  is the electron velocity distribution function,  $\mathbf{c}$  is the vector electron velocity,  $\nabla_x$  is the gradient operator with respect to positional space, and  $\nabla_c$  is the gradient in velocity space. The EVDF  $f$  is separated into a component that is predominantly isotropic,  $f_0$ , and components that skew the distribution in the directions of the electric field and the  $\mathbf{E} \times \mathbf{B}$  drift [11, 12]:

$$f(\mathbf{c}) = f_0(c) + (\mathbf{c} \cdot \mathbf{E}) f_1(c) + [\mathbf{c} \cdot (\mathbf{B} \times \mathbf{E})] f_2(c). \quad (2)$$

The functions  $f_1$  and  $f_2$  are also isotropic, and when weighted by  $cE$  and  $c(\mathbf{B} \times \mathbf{E})$ , result in small perturbations on the predominantly isotropic core. Therefore, this model may not be appropriate for EVDFs with extreme anisotropy due to high drift energies or “beam-like” electrons streaming from the cathode neutralizer, e.g. [9]. We will not address the

anisotropy of the EVDF in this paper. When an EVDF found from this form of the Boltzmann equation is converted to an EEDF by averaging over all directions, the anisotropic components vanish (see Appendix A.).

The directions of the electric field  $\mathbf{E}$  and magnetic field  $\mathbf{B}$  are taken as purely axial ( $\mathbf{z}$ ) and radial ( $\mathbf{r}$ ), respectively. We then neglect spatial gradients in the axial direction by making the ‘‘local field’’ approximation. The cyclotron radius of the electrons in the Hall discharge is 10-1000 times smaller than the electron mean-free-path, except very near the anode. Thus, the EEDF is formed locally, at distances below the mean-free-path. In other words, due to magnetic confinement, an electron reaches equilibrium with the local fields on time scales shorter than that which controls diffusion across a characteristic length scale of the plasma. The axial variation of the EEDF is determined solely by the axial change in plasma properties. This approach has been successfully applied to the determination of the EEDF in a cylindrical magnetron [13], a discharge similar to the Hall thruster in size, pressure, and magnetic field-strength. We also treat the plasma as uniform in the azimuthal direction due to symmetry, and in the radial direction, as electrons can freely diffuse along radial magnetic field lines. For a more detailed explanation of the local and non-local approaches to solving the Boltzmann equation, see [14].

After removing the spatial gradient term, the solution proceeds by substituting the perturbation expression Eq. (2) into Eq. (1), expanding the right-hand-side as a series of collision integrals, and simplifying the equation to a scalar expression for the isotropic EVDF  $f_0$ . This laborious procedure is detailed for elastic collisions only in [12] and for elastic and inelastic collisions in [11] and will not be repeated here.

For this study, we restrict the inelastic collisions to ionization and wall-loss collisions and their corresponding secondary electron processes. Other inelastic electron-neutral collisions, as well as electron-electron and electron-ion collisions, have been neglected. The temperature of the background xenon neutrals is also neglected. These details may be added to the model in a later study. We convert from speed to kinetic energy using  $u=kc^2$ , where the constant  $k$  is defined such that  $u$  is expressed in eV.

The subscript is also dropped from the isotropic EVDF  $f_0$ , and we have let  $f(c) = f(u)$  for convenience. After adding the wall-loss collisions and separating the elastic and inelastic terms, the equation becomes

$$\frac{4}{3} \left( \frac{eE}{m} \right)^2 k^2 \frac{d}{du} \left[ \left( \frac{N\sigma_m u^2}{k\omega^2 + N^2\sigma_m^2 u} \right) \frac{df}{du} \right] + N \frac{2m}{M} \frac{d}{du} [u^2 \sigma_m f] = \quad (3)$$

$$uN\sigma_i(u)f(u) - N(u+u_i)\sigma_i(u+u_i)f(u+u_i) + \sqrt{k}u v_{wall}(u)f(u).$$

Here,  $N$  is the neutral gas density,  $m$  and  $M$  are the electron and xenon atom masses, respectively,  $\omega$  is the electron cyclotron frequency,  $\sigma_m$  is the momentum-transfer cross-section for electron-neutral collisions,  $\sigma_i$  is the cross-section for ionization, and  $u_i$  is the threshold energy for ionization.

From left to right, the terms in the equation represent Joule heating, elastic collisions, loss of electrons due to ionization, return of electrons from ionizing collisions, and loss of electrons to the wall. Equation (3) assumes that electrons are transported across the magnetic field lines primarily by elastic collisions with xenon atoms. Alternatively, an *ad hoc* experimentally-determined ‘‘effective’’ collision frequency can be used by substituting  $v_{eff}$  for  $N\sigma_m c$  in the derivation. The effective collision frequency attempts to include effects left out by this model, such as electron-wave interactions. These two momentum-transport models will be compared later in the paper.

### Secondary Electrons from Ionization

In Eq. (3), ionization and wall-loss are treated as inelastic excitation collisions that do not produce electrons. At this point, we introduce secondary electron terms to the model, following [15]. We start by deriving the contribution to the EEDF of secondary electrons produced by ionization. The expressions derived here will be modified to describe secondary electrons from the wall later in the paper. We define  $q$  as the cross-section for producing secondary or scattered electrons of particular energies. The collision term for ionization is then expressed as

$$\left( \frac{\delta f(u)}{\delta t} \right)_{coll.} = \frac{cN}{u} \int_{2u+u_i}^{\infty} u' q_{sec}^i(u', u) f(u') du' \quad (4)$$

$$+ \frac{cN}{u} \int_{u+u_i}^{2u+u_i} u' q_{sca}^i(u', u) f(u') du' - cN\sigma_i(u)f(u).$$

The first two terms on the right-hand-side are the source terms for secondary and scattered electrons, respectively. The third term is the ionization loss term.

The variable  $u'$  is a dummy variable of integration. The integrals involving  $q$  can be simplified using delta-function expressions:

$$\begin{aligned} q_{sec}^i(u', u) &= \sigma_I(u') \delta(u - \tilde{u}), \quad \text{and} \\ q_{sca}^i(u', u) &= \sigma_I(u') \delta[u - (u' - u_I - \tilde{u})]. \end{aligned} \quad (5)$$

Here,  $\delta$  is the Dirac delta function, and  $\tilde{u}$  is the energy of the secondary electron. The value

$$\tilde{u} = \left( \frac{u' - u_I}{2} \right), \quad (6)$$

representing a case in which the energy remaining from the inelastic collision is divided equally between the secondary and scattered electrons, is used here. Combining Eqs. (4)-(6) and substituting into Eq. (3), we arrive at

$$\begin{aligned} \frac{4}{3} \left( \frac{eE}{m} \right)^2 k^2 \frac{d}{du} \left[ \left( \frac{N\sigma_m u^2}{k\omega^2 + N^2\sigma_m^2 u} \right) \frac{df}{du} \right] + N \frac{2m}{M} \frac{d}{du} [u^2 \sigma_m f] = \\ uN\sigma_I(u) f(u) - 2N(2u + u_I)\sigma_I(2u + u_I) f(2u + u_I) + \sqrt{ku} v_{wall}(u) f(u). \end{aligned} \quad (7)$$

### Electron-wall interaction

To complete Eq. (7), we must describe the details of the electron-wall interaction and add the secondary electrons from the wall. The wall scattering collision frequency  $\nu_{wall}$  must take into account both the transit-time of electrons in the discharge channel and the sheath formed at the channel wall. We write the characteristic rate at which an electron of velocity  $c$  reaches the wall as  $c/w$ , where  $w$  is the (radial) width of the discharge channel. Since the magnetic field lines are almost radial and the mean-free-path is on the order of the channel width, electrons are free to stream to the wall; however, only electrons with energies greater than the wall-sheath potential will actually reach the wall. Electrons of lower energy should scatter off the sheath elastically and specularly. So, the final expression for the rate of wall scattering is

$$\nu_{wall} = H(u - e\phi_{wall}) \frac{c}{w} = H(u - e\phi_{wall}) \frac{1}{w} \sqrt{\frac{u}{k}}, \quad (8)$$

where  $H$  is the Heaviside step-function and  $\phi_{wall}$  is the magnitude of the (negative) sheath potential. The calculation of the sheath potential will be described later in the paper.

We can apply the same formalism used for secondary electrons from ionization to wall collisions. Here, we

introduce the phenomenological model for electron scattering used by Degond *et al.* [7]. Although there is little physical basis for the exact form of this model, it is nonetheless more general than the one used in our previous study [10]. The total rate of electron scattering from the wall is given by

$$\nu_{tot} = \nu_{wall}(u) \gamma^\dagger(u - e\phi_{wall}). \quad (9)$$

Here,  $\gamma^\dagger(\varepsilon)$  is the experimentally-determined secondary electron emission coefficient ( $\gamma$  is used to avoid confusion with the Dirac delta function), which generally takes the form [16, 17]

$$\gamma^\dagger(\varepsilon) = \left( \frac{\varepsilon}{\varepsilon_1} \right)^p. \quad (10)$$

For our purposes, we define any electron that returns from the wall to be a secondary electron. As in the previous paper [10], we approximate the form of  $\gamma^\dagger(\varepsilon)$  as linear, i.e.,  $p=1$ .

The electrons returned from the wall are split into two populations—electrons that have scattered elastically and diffusely off the microscopically rough wall, and low energy “true secondaries” knocked out of the wall lattice. The first-crossover energy  $\varepsilon_1$ , defined by  $\gamma^\dagger(\varepsilon_1)=1$ , is treated as a threshold for the production of true secondaries. Electrons hitting the wall with energies less than  $\varepsilon_1$  can only be scattered elastically. This leads to simple expressions for  $\gamma_e$  and  $\gamma_s$ , the coefficients of elastically scattered electrons and true secondary electrons, respectively,

$$\gamma_e = \begin{cases} \gamma^\dagger(u - e\phi_{wall}), & u - e\phi_{wall} < \varepsilon_1 \\ 2 - \gamma^\dagger(u - e\phi_{wall}), & \varepsilon_1 < u - e\phi_{wall} < \varepsilon_2 \\ 0, & u - e\phi_{wall} > \varepsilon_2 \end{cases} \quad (11a)$$

and

$$\gamma_s = \begin{cases} 0, & u - e\phi_{wall} < \varepsilon_1 \\ \gamma^\dagger(u - e\phi_{wall}) - \gamma_e(u - e\phi_{wall}), & \varepsilon_1 < u - e\phi_{wall} < \varepsilon_2 \\ \gamma^\dagger(u - e\phi_{wall}), & u - e\phi_{wall} > \varepsilon_2 \end{cases}, \quad (11b)$$

where  $\varepsilon_2$  is defined by  $\gamma^\dagger(\varepsilon_2)=2$ . The various scattering coefficients are shown in Fig. 1 for  $p=1$ .

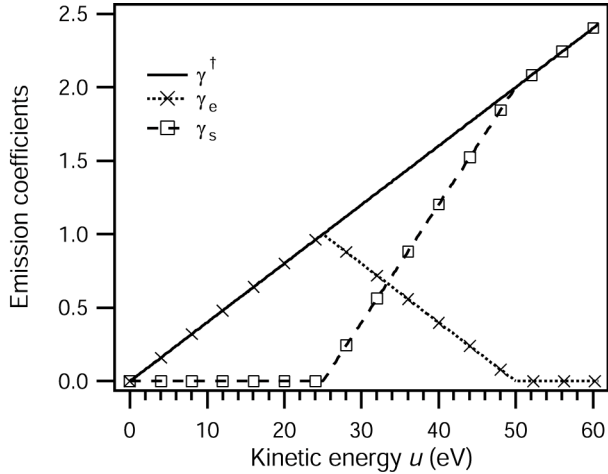


Figure 1-Secondary electron emission coefficients, from Eqs. (10) and (11) with  $p=1$  and  $\varepsilon_1=25$  eV.

The form for  $\gamma^\dagger(\varepsilon)$  in [7] was slightly modified so that  $\gamma^\dagger(\varepsilon) \rightarrow 2$  as  $\varepsilon \rightarrow \infty$ , eliminating the need for the third energy range in Eq. (11). In this case, the boundary condition  $\gamma_e(\varepsilon)=0$ ,  $\varepsilon > \varepsilon_2$  is admittedly arbitrary; however, the number of secondary electrons formed above  $\varepsilon_2$  is so small that this makes little difference.

To complete the boundary conditions at the wall, we assume that true secondary electrons return to the plasma with negligible energy, i.e.,  $\tilde{u}=0$ . Electrons returned from the wall to the bulk plasma should at least regain the wall potential energy ( $\tilde{u}=e\phi_{wall}$ ); however, the total number of secondary electrons produced is small enough that this effect is negligible. Evaluating Eqs. (8)-(11) in the formalism of Eqs. (4) and (5), we get the total contribution of wall collisions to the EEDF:

$$\left(\frac{\delta f(u)}{\delta t}\right)_{loss} = (1-\gamma_e(u-e\phi_{wall}))v_{wall}(u)f(u) \quad (12a)$$

and

$$\left(\frac{\delta f(u)}{\delta t}\right)_{sec.} = \frac{1}{\sqrt{u}}\delta(u)\int\sqrt{u'}\gamma_s(u'-e\phi_{wall})v_{wall}(u')f(u')du' \quad (12b)$$

Since the elastically scattered electrons lose no energy, they effectively reduce the wall-loss. In the previous paper [10], we had assumed that all electrons striking the wall are lost, i.e.,  $\gamma_e \equiv 0$ .

Inserting Eq. (12) into Eq. (7), we get,

$$\begin{aligned} & \frac{4}{3}\left(\frac{eE}{m}\right)^2 k^2 \frac{d}{du}\left[u^{\frac{3}{2}}\left(\frac{v_{eff}}{v_{eff}^2+\omega^2}\right)\frac{df}{du}\right] + N\frac{2m}{M}\frac{d}{du}\left[u^2\sigma_m f\right] \\ & = Nu\sigma_i(u)f(u) - 2N(2u+u_i)\sigma_i(2u+u_i)f(2u+u_i) \quad (13a) \\ & + \frac{u}{w}(1-\gamma_e(u-e\phi_{wall}))H(u-e\phi_{wall})f(u) \\ & - \delta(u)\int_{e\phi_{wall}}^{\infty}\frac{u'}{w}\gamma_s(u'-e\phi_{wall})f(u')du'. \end{aligned}$$

The ionization return-term represents two electrons at equal energies. The wall-secondary term is equivalent to returning all secondary electrons from the wall to the EVDF at zero energy. We have also made the substitution  $v_{eff}$  for  $N\sigma_m c$  in the derivation, which will be justified later in the paper. The equation must satisfy one boundary condition at infinity,

$$f \rightarrow 0 \text{ as } u \rightarrow \infty, \quad (13b)$$

and the normalization condition,

$$\int_0^{\infty}\sqrt{u}fdu = \int_0^{\infty}Fdu = 1. \quad (13c)$$

### Wall-sheath potential

The wall-sheath potential is calculated from an electron balance, so a detailed sheath model is unnecessary. Electron production by ionization is balanced by the net outflow of electron current and the net loss of electrons to the wall:

$$\begin{aligned} & \frac{n_e A_{chan}}{\sqrt{k}} \int_0^{\infty} Nu\sigma_i(u)f(u)du - \frac{1}{e}\frac{dI_e}{dz} \\ & = \frac{n_e A_{chan}}{\sqrt{k}} \int_{e\phi_{wall}}^{\infty} \frac{u}{w}(1-\gamma^\dagger(u-e\phi_{wall}))f(u)du, \end{aligned} \quad (14)$$

where  $A_{chan}$  is the cross-sectional area of the discharge channel. The equation must be solved iteratively in order to self-consistently determine the wall-potential from the calculated EEDF and the experimental input data. The details of the iteration and the numerical method used are given in Appendix B.

### Inputs

The Boltzmann equation takes as inputs plasma properties derived from optical and probe experiments performed on a laboratory Hall thruster with an alumina ( $Al_2O_3$ ) channel. In total, solution of Eq. (13) requires, as a function of the axial coordinate  $z$ , the

electric field  $E$ , magnetic field  $B$ , neutral xenon density  $N$ , and effective collision frequency  $\nu_{eff}$ . The electron density  $n_e$  and electron current  $I_e$  are also needed to find the wall-sheath potential. These data are summarized in [18]. Details of the experiments can be found in [19, 20]. For these experiments, the thruster was operated with a peak magnetic field-strength of 120 G and a mass flow rate of 2 mg/s xenon. Cross-section data were taken from the SIGLO database [21]. We approximated the secondary electron-emission coefficient for alumina as linear, with a first crossover energy of  $\varepsilon_1 = 25$  eV [22].

### Model Summary

The electron Boltzmann equation is reduced to an ordinary differential equation in kinetic-energy space. The EEDF at any position in the channel is determined only by the local plasma properties—there is no diffusion in positional space. Elastic gas-phase collisions, ionization collisions, and wall collisions are included in the model. The momentum-transfer collision frequency is calculated using either a cross-section or an experimentally determined effective mobility. Secondary electrons from ionization and/or from wall collisions can be included. Only electrons with energy greater than the local wall-sheath potential can be lost to the wall. Electrons returned from the wall are split into two populations—elastically (diffusely) scattered electrons, and true, low-energy secondary electrons. The resultant equation is solved iteratively, with the wall-sheath potential calculated at each iteration from a local electron balance.

## Results

### General results

Figure 2 shows the isotropic part of the EVDF  $f$  calculated using the effective collision frequency for momentum transfer for 200 V operation, 15 mm upstream of the thruster exit. Elastic, diffuse electrons from the walls are also neglected, i.e.,  $\gamma_e \equiv 0$  in Eq. (11). For ionization collisions only (no secondaries, no wall), the EVDF is nearly Maxwellian, except near zero energy. Including secondary electrons from ionization (no wall) results in more low-energy electrons in the distribution, decreasing the average energy. When wall-collisions are added to the model (no secondaries & All effects), the average energy

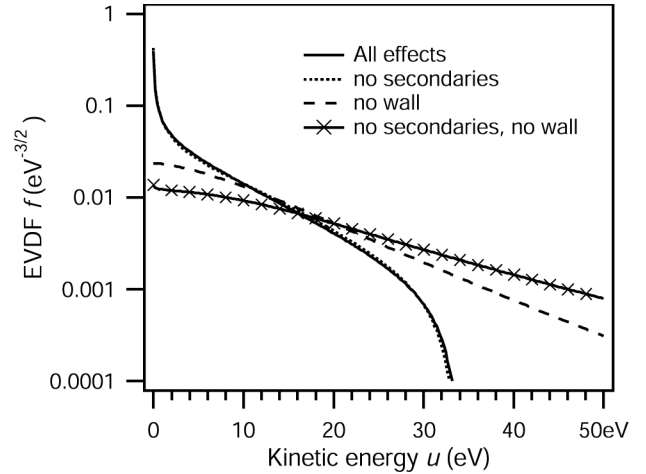


Figure 2-Calculated EVDFs  $f$  for various inelastic processes.

decreases dramatically. At energies beyond the wall-sheath potential ( $\sim 30$  V for this case), the distribution falls off quickly as electrons are lost to the wall.

Surprisingly, re-injecting secondary electrons from the wall has no visible effect on the distribution. This fact is more apparent in Fig. 3, where the EEDF  $F = \sqrt{u}f$  is plotted for the same conditions. While including wall-secondaries has little effect, including secondary electrons from ionization does noticeably change the distribution. This is because ionization produces more secondary electrons in the plasma than does wall-loss. As shown in Fig. 4, the ionization rate is greater than the wall-loss rate throughout most of the channel.

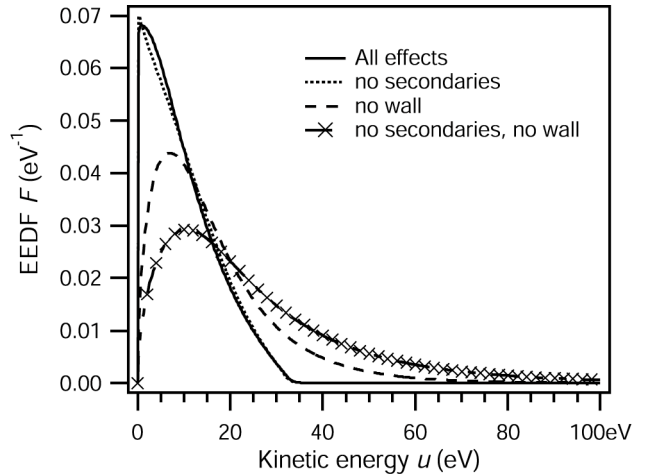


Figure 3-Calculated EEDFs  $F$  for various inelastic processes.

### Momentum-transfer models

Figure 4 compares all the collision-frequencies used or generated by the code. Here,  $\nu_I$  and  $\nu_m$  are the frequencies for ionization and elastic momentum-transfer collisions, respectively, as calculated using the SIGLO cross-sections;  $\nu_{wall}$  is the bulk rate of wall-loss collisions, given by integrating Eq. (7) over  $F$ ;  $\nu_S = \nu_m + \nu_I + \nu_{wall}$  is the total collision frequency; and  $\nu_{eff}$  is the experimentally determined effective collision frequency. Elastic collisions with xenon neutrals dominate inelastic processes throughout the channel. It seems unlikely that wall-loss collisions and secondary electrons contribute greatly to electron momentum transfer in the discharge, at least at the operating conditions investigated here.

Near the anode, elastic collisions are clearly sufficient for electron momentum transfer in the discharge; however, within 30 mm of the thruster exit, elastic collisions cannot account for the measured cross-field electron transport. It is worth noting that the trend in  $\nu_m$  with  $z$  is due almost entirely to the neutral gas density  $N$ , which was measured with great experimental uncertainty. The dip in  $\nu_{eff}$  at  $z = -10$  is less severe at other discharge operating conditions and is, as of yet, unexplained.

The differences between the two momentum models used for this study, i.e.,  $\nu_m = \nu_{eff}$  vs.  $\nu_m = N\sigma_m c$ , is also evident in Fig. 5. The EVDF calculated using  $\nu_{eff}$  (for 200 V operation 15 mm upstream of the exit) agrees very well with a Maxwellian distribution at the

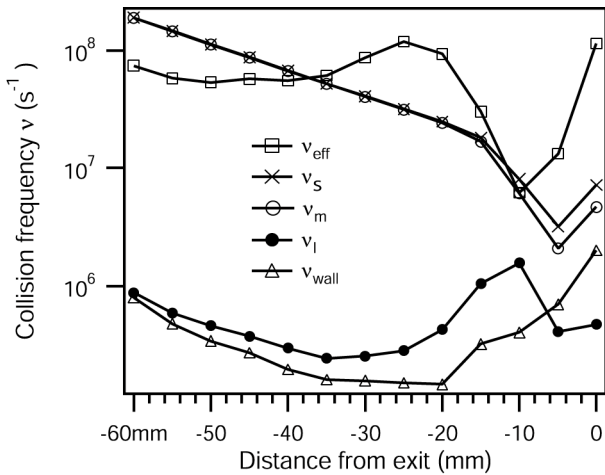


Figure 4-Comparison of various collision frequencies inside the thruster channel at 200 V operation.

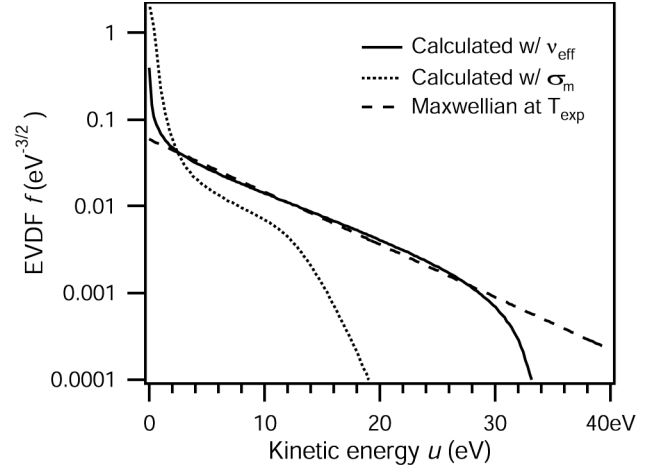


Figure 5-Calculated EVDFs for different momentum-transfer models and comparison to Maxwellian distribution.

experimental electron temperature,  $T_{exp}$ , even though the plasma properties used as inputs to the model depend very weakly on  $T_{exp}$ . Using only elastic collisions for momentum transport, the model cannot suitably reproduce the experimentally-observed electron temperature. Therefore, we use  $\nu_m = \nu_{eff}$ , as in Eq. (13a), for the remainder of the EEDF calculations in this paper.

### Comparison to experiment

A closer look at Fig. 5 shows that the calculated EVDF agrees very well with a Maxwellian at  $T_{exp}$  at intermediate energies (15-30 eV), but deviates at extreme energies. Thus, the calculated distribution has a slightly lower mean energy than experiments suggest. This is better seen in Fig. 6, a comparison between the experimental and calculated electron temperatures, where the effective temperature is defined as that of a Maxwellian distribution with the same mean energy,

$$\bar{u}_{Max} = \frac{3}{2} k_B T_e \rightarrow k_B T_{eff} = \frac{2}{3} \bar{u} = \frac{2}{3} \int_0^{\infty} u F du \quad (15)$$

Near the exit plane, the temperatures agree fairly well. The fact that the experimental electron temperature is reproduced within a few electron volts suggests that we have correctly formulated the energy gain and loss terms in the Boltzmann equation. The large discrepancies near the anode are possibly due to error in the neutral gas density  $N$ , as mentioned above.

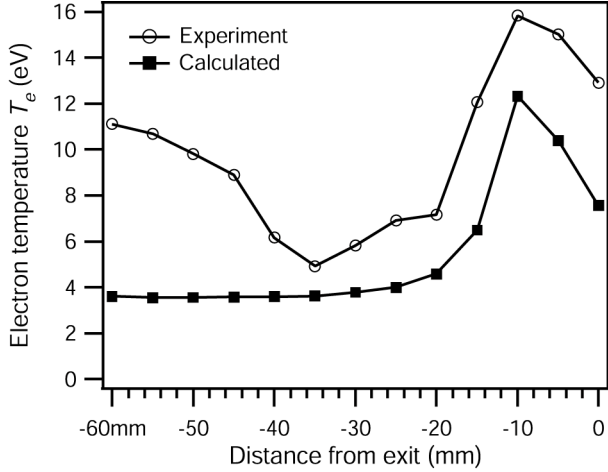


Figure 6-Comparison of calculated and measured electron temperatures.

### Elastic wall scattering

In Fig. 7, we investigate the impact of splitting the returned electron population into two populations, i.e.,  $\gamma_e \neq 0$  in Eq. (11). The effective collision frequency is used for momentum transfer in this comparison. When some electrons are allowed to return elastically from the wall, we see a second “hump” in the EEDF. The hump occurs because these elastic electrons effectively decrease the wall loss rate (see Eq. (12)). The EEDF turns downward again when  $u - e\phi_{wall} > \varepsilon_1$ . Beyond this energy, the number of elastically reflected electrons decreases.

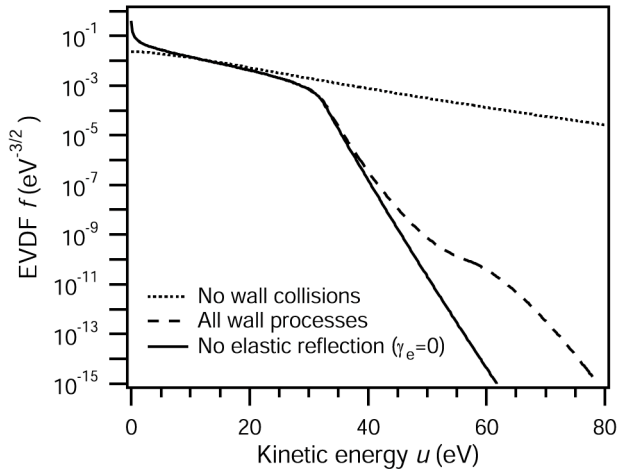


Figure 7-Calculated EVDFs  $f$  for different secondary electron models for 200 V operation, 15 mm upstream of the thruster exit.

The shape of the hump is determined solely by the specific forms of the secondary electron emission coefficients. Thus, the energy of the second hump is determined by the local wall potential and is unrelated to near-wall conductivity. It is worth restating that the secondary electron model used here is purely phenomenological. If different expressions were used for the secondary emission coefficients were used, e.g., if  $\gamma_e$  and  $\gamma_s$  were both allowed to increase with energy, the hump would not form. Regardless, the value of  $f$  at the second hump is so low that it has virtually no impact on any collision rates calculated from the EEDF. Nonetheless, it is interesting that the “double-hump” distribution can be generated in models by a variety of different mechanisms.

### Wall sheath potential

The EEDF simulation can also be used to compare the calculated wall-sheath potential and wall-loss rates to other sheath models. The wall-sheath potential, is generally found by balancing the net flux of electrons and ions to the wall [23, 16, 17]. Assuming the ions enter the sheath at the Bohm velocity, this balance yields,

$$(1 - \gamma_{eff}) \frac{\bar{c}_e}{4} n_e \exp\left(\frac{e\phi_{wall}}{kT_e}\right) = n_e \sqrt{\frac{k_B T_e}{M}}. \quad (16)$$

Here,  $\gamma_{eff}$  is the effective secondary-emission-coefficient, defined by,

$$\gamma_{eff} = \frac{\Gamma_{secondary}}{\Gamma_{primary}} \quad (17)$$

The coefficient is generally found by computing the one-way-flux of a Maxwellian distribution multiplied by the function  $\gamma(u)$ ,

$$\gamma_{eff} = \frac{\int_{-\infty}^{\infty} \int_{-\infty}^{\infty} \int_0^{\infty} \gamma(u) c_1 f_{MB}(\bar{c}) d\bar{c}}{\int_{-\infty}^{\infty} \int_{-\infty}^{\infty} \int_0^{\infty} c_1 f_{MB}(\bar{c}) d\bar{c}}, \quad (18)$$

where  $f_{MB}(\bar{c})$  is the Maxwell-Boltzmann velocity distribution about the electron temperature  $k_B T_e$ . No differentiation between elastically scattered and true secondaries is necessary for calculating the wall potential, so we drop the superscript  $\dagger$  for convenience.

For a linear  $\gamma$  (Eq. (10) with  $p=1$ ), this leads to

$$\gamma_{eff} = \frac{2k_B T_e}{\varepsilon_1}, \quad (19)$$

where  $\varepsilon_1$  is the first cross-over energy of the material; however, as mentioned above, the secondary emission coefficient should really be evaluated at the energy of the electron after it has been decelerated by the sheath, i.e.,  $\gamma(u - e\phi_{wall})$ :

$$\gamma_{eff} = \frac{\int_{-\infty}^{\infty} \int_{-\infty}^{\infty} \int_{c_0}^{\infty} \gamma(u - e\phi_{wall}) c_1 f_{MB}(\bar{c}) d\bar{c},}{\int_{-\infty}^{\infty} \int_{-\infty}^{\infty} c_1 f_{MB}(\bar{c}) d\bar{c}}, \quad (20)$$

where the lower-bound velocity in the perpendicular ( $c_1$ ) direction is equivalent to the wall potential energy.

It turns out that for a linear  $\gamma$ , Eqs. (18) and (20) give the same result—the effective secondary coefficient is independent of the wall-sheath potential. Therefore, the flux balance in Eq. (16) can be solved explicitly for the wall-sheath potential:

$$\phi_{wall} = -\frac{k_B T_e}{e} \ln \left[ \left( 1 - \frac{2k_B T_e}{\varepsilon_1} \right) \sqrt{\frac{M}{2\pi m}} \right] \quad (21).$$

As  $k_B T_e \rightarrow \varepsilon_1/2$  and  $\gamma_{eff} \rightarrow 1$ , the sheath is neutralized by secondary electrons and collapses. This effect brings down the sheath potential at high temperature,

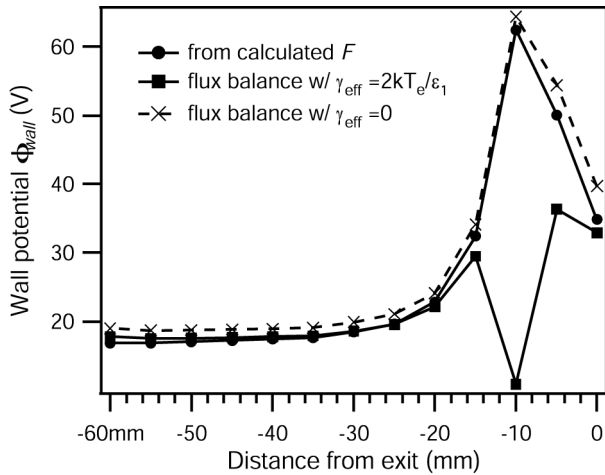


Figure 8-Comparison of wall potential models.

severely increasing the predicted rate of electron loss to the wall. Eventually, the sheath reaches space-charge saturation [16, 17]. Under this condition,  $\gamma_{eff} \approx 1$  and the magnitude of the (still negative) sheath potential increases approximately linearly with temperature [17].

In Fig. 8, the wall-sheath potential returned by the Boltzmann equation simulation is compared to Eq. (21) using the calculated electron temperature of Eq. (15). The sheath model shows excellent agreement with the simulation except for two points near the discharge exit. At these two points, the sheath is partially neutralized, but has not reached space-charge saturation. The discrepancy is due to overestimating the effective secondary emission coefficient. When Eq. (21) is used with  $\gamma_{eff} = 0$ , agreement is quite good.

To explore this further, we compare the rates of wall-loss and wall-return predicted by the EEDF simulation to those of a Maxwellian distribution of the same average energy. From above,

$$v_{wall} = \frac{\bar{c}_e}{w} \exp\left(\frac{-e\phi_{wall}}{kT_{eff}}\right) \quad (22a)$$

$$\text{and } v_{secondary} = \frac{2kT}{\varepsilon_1} \frac{\bar{c}_e}{e w} \exp\left(\frac{-e\phi_{wall}}{kT_{eff}}\right) \quad (22b)$$

for the Maxwellian distribution, whereas we use

$$v_{wall} = \frac{1}{\sqrt{k}} \int_{e\phi_{wall}}^{\infty} \frac{u}{w} f(u) du \quad (23a)$$

$$\text{and } v_{secondary} = \frac{1}{\sqrt{k}} \int_{e\phi_{wall}}^{\infty} \frac{u}{w} \gamma^\dagger(u - e\phi_{wall}) f(u) du \quad (23b)$$

for the calculated EEDF. Figure 9 shows that both the wall-loss and wall-return rates predicted with a Maxwellian ( $f_{MB}$ ) are quite high. For the Maxwellian case, the secondary electron flux is almost equal to the primary flux near the channel exit, where the sheath approaches charge saturation. The wall-return rate actually exceeds the experimental effective collision frequency for momentum transfer  $\nu_{eff}$ . If the EEDF were Maxwellian, we would expect electrons returned from the wall to significantly contribute to cross-field transport.

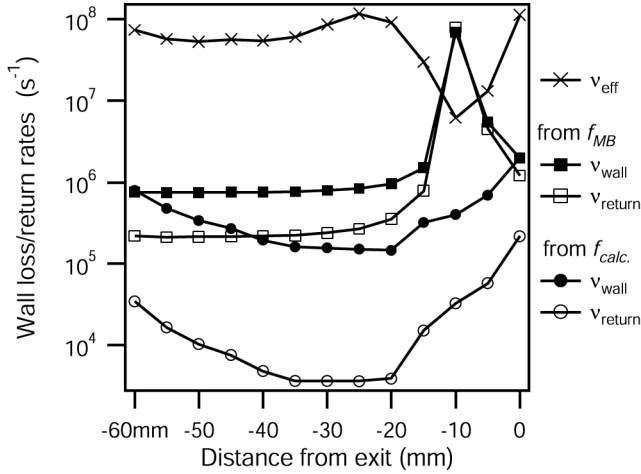


Figure 9-Comparison of wall-loss models.

On the other hand, the wall-loss rate calculated in the EEDF simulation ( $f_{calc.}$ ) is much lower than those predicted by a Maxwellian. The wall-return rate is even lower and is never comparable to  $v_{eff}$ . The effective secondary emission coefficient, defined here as  $\gamma_{eff} = v_{secondary}/v_{wall}$ , is plotted in Fig. 10. The fraction of electrons returning from the wall is much lower for the calculated EEDF than for the Maxwellian case, so the wall-sheath never approaches charge saturation.

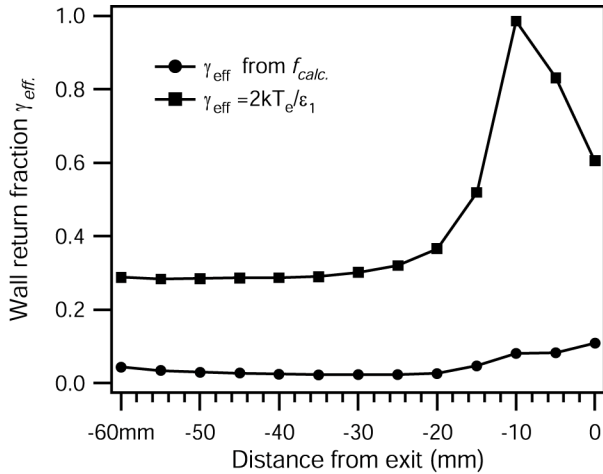


Figure 10-Effective secondary emission coefficient.

In the previous paper [10], we speculated that charge saturation is avoided in the EEDF simulation because the secondary emission coefficient is evaluated at the kinetic energy less the wall potential energy; however, as mentioned above, this shift does not change the

results for a Maxwellian distribution. The difference is attributable solely to the non-Maxwellian shape of the EEDF.

### Rough Sheath

There is another mechanism by which the electron-wall interaction can contribute to cross-field transport. The ceramic walls of a Hall thruster have some finite roughness. At some short distance from the wall, we would expect the structure of the wall sheath to deviate from 1-D and take on this roughness. This idea was also considered by Morozov. An electron with energy slightly below the wall-potential may penetrate to this “rough sheath” and scatter off of it in a non-specular way. This interaction would be nearly elastic, so the electron could change direction without losing much energy. This kind of collision would play the same role as the elastic/diffuse secondary electrons described above. Since the EEDF drops off sharply near the wall potential, many more electrons will make it part-way through the sheath than will make it all the way to the wall.

We can use a simple model for the sheath structure to estimate the sheath roughness necessary to make this effect significant. In the absence of charge-saturation, the sheath structure can be approximated as exponential,

$$\phi(x) = \phi_{wall} e^{-x/\lambda_D}, \quad (24)$$

where  $x$  is the perpendicular distance from the wall and  $\lambda_D$  is the Debye length based on the average temperature of the calculated EEDF. We can calculate the number of electrons penetrating the sheath to distance  $x$  from the wall by using Eq. (23a) with  $\phi(x)$  instead of  $\phi_{wall}$ . We will consider this mechanism to be significant when the wall-collision frequency is half of the effective collision frequency for momentum transport,  $v_{eff}$ . Figure 11 shows a plot of the distance from the wall at which this occurs for 200 V operation, calculated by solving Eq. (24) for  $x$ . This plot shows that while the frequency of electrons penetrating the entire sheath can be quite small, the number of electrons getting to within 5-30  $\mu\text{m}$ . of the wall can be very large. Oscillations in the sheath potential may also be important to this form of scattering. Further work is needed to explore this mechanism for near-wall conductivity.

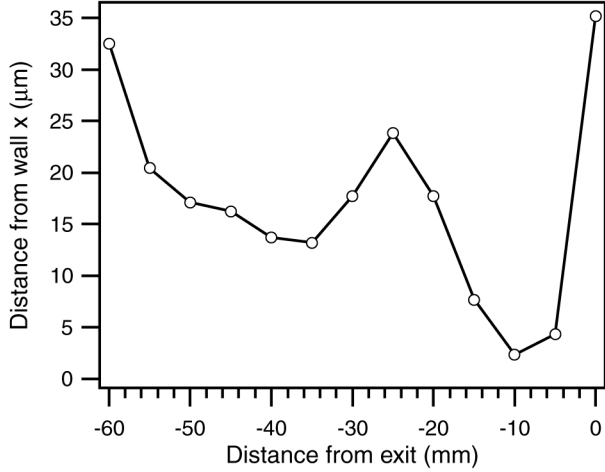


Figure 11-Distance from wall at which  $v_{wall} = v_{eff} / 2$ .

## Conclusions

We can draw several conclusions from the results of this study. Obviously, electron-wall collisions play a critical role in the discharge energy balance. By selectively removing high energy electrons from the distribution, wall-collisions significantly lower the mean electron energy and, combined with ionization, skew the distribution towards low energies. At intermediate energies between the wall-sheath potential and the ionization threshold, the EEDF behaves essentially like a Maxwellian distribution; however, assuming a Maxwellian distribution for the electrons is generally not acceptable. Our results suggest that models of the electron-wall interaction must account for the shape of the EEDF. Compared to the Boltzmann equation model, a Maxwellian distribution over predicts the wall-loss and wall-return rates. This is a critical for studying near-wall conductivity. The wall-return rate calculated from this Boltzmann equation model is too low to significantly contribute to cross-field transport.

An additional, unforeseen result of this study was a new potential mechanism for forming the second hump of a double-hump EEDF. Since the model that led to formation of this hump has little physical basis, we do not think this mechanism is correct. Nonetheless, it underscores the difficulty of speculating on the exact EEDF-formation mechanism (or combination of mechanisms) from experimental results. To fully tackle this problem, we need a much better physical understanding of all the processes controlling the electron-wall interaction.

## Future Work

The Boltzmann-solver EEDF model developed here can be improved in several ways. The first way to improve the model's accuracy is simply to include more terms in the initial equation (3). Expressions for electron-electron and electron-ion collisions [24] and for spatial diffusion [14] can be added to Eq. (3) without significantly increasing the complexity of the numerical solution. Inelastic collisions other than ionization could also be added, as several cross-sections are readily available for xenon [21]. Of course, the equation could be improved by retaining the time-dependent terms and the spatial gradient terms. We also plan to continue to use this model in conjunction with a hybrid fluid-PIC simulation (with no feedback) to study the EEDFs for operating conditions and wall materials that have not been explored experimentally.

## Acknowledgments

This work was sponsored by the Air Force Office of Scientific Research. The authors would like to thank N. Gascon, M. Dudeck, S. Barral, A. A. Ivanov, M. Bacal, and G. Karabadzhak for helpful discussions on electron kinetics and electron-wall interactions, and P. Degond for providing a pre-print version of the excellent paper [8].

## Appendix

### A. Anisotropy

Equation (2) can be used to calculate the complete EVDF in velocity space from the calculated isotropic core  $f_0$ . Following Sutton and Sherman [12], equation (2) can be re-written as

$$f_e(\mathbf{c}) = f_0(c) + \frac{e}{m} [c_1 E f_1 + c_2 E B f_2], \quad (\text{A1})$$

where  $c_1$  is in the axial ( $\mathbf{E}$ ) direction and  $c_2$  is in the azimuthal ( $\mathbf{E} \times \mathbf{B}$ ) direction. The isotropic perturbation functions are given by

$$f_1 = \frac{v}{c(\omega^2 + v^2)} \frac{df_0}{dc} \quad (\text{A2})$$

$$\text{and } f_2 = \frac{e}{mc(\omega^2 + v^2)} \frac{df_0}{dc}. \quad (\text{A3})$$

To get the distribution  $f_e$  in speed space, we can convert  $f_e dc_1 dc_2 dc_3$  to spherical coordinates and integrate over the angular variables. This requires the following transformations:

$$\begin{aligned} c_1 &= c \sin \theta \sin \phi; & c_2 &= c \sin \theta \cos \phi; & c_3 &= c \cos \theta \\ dc_1 dc_2 dc_3 &= c^2 \sin \theta dc d\theta d\phi \\ \theta &\in [0, \pi]; & \phi &\in [0, 2\pi] \end{aligned} \quad (\text{A4})$$

Substituting Eqs. (A2)-(A4) into Eq. (A1) and integrating over  $\phi$  and  $\theta$  gives

$$\begin{aligned} f_{\text{speed}}(c) &= c^2 f_0 \int_0^\pi \sin \theta d\theta \int_0^{2\pi} d\phi \\ &+ \frac{eE}{m} c^3 f_1 \int_0^\pi \sin^2 \theta d\theta \int_0^{2\pi} \sin \phi d\phi \\ &+ \frac{eEB}{m} c^3 f_2 \int_0^\pi \sin^2 \theta d\theta \int_0^{2\pi} \cos \phi d\phi \end{aligned} \quad (\text{A5})$$

Scalar constants and the isotropic functions  $f$  and  $c$  have been removed from the directional integrals. By inspection, the second two terms on the right-hand-side of Eq. (A5) are zero, as the integrals over  $\phi$  vanish. Thus, the perturbation terms in the full EVDF do not appear in speed space or energy space.

## B. Numerical Solution

### Collision Operators

It is convenient to re-write Eq. (13a) using collision operators before proceeding with the numerical solution [13]:

$$D(u) = \frac{4}{3} \left( \frac{eE}{m} \right)^2 k^2 \left( \frac{N \sigma_m u^2}{k \omega^2 + N^2 \sigma_m^2 u} \right) \quad (\text{B1a})$$

for electron transport by elastic collisions only, or

$$D(u) = \frac{4}{3} \left( \frac{eE}{m} \right)^2 k^{\frac{3}{2}} u^{\frac{3}{2}} \left( \frac{v_{\text{eff}}}{v_{\text{eff}}^2 + \omega^2} \right) \quad (\text{B1b})$$

for an experimental (energy-independent) collision-frequency. Similarly,

$$G(u) = N \frac{2m}{M} u^2 \sigma_m, \quad \text{or} \quad (\text{B2a})$$

$$G(u) = \frac{2m}{M} k^{\frac{1}{2}} u^{\frac{3}{2}} v_{\text{eff}}. \quad (\text{B2b})$$

$$J(u) = Nu \sigma_i(u), \quad (\text{B3})$$

$$W(u) = \frac{u}{w} (1 - \gamma_e(u - e\phi_{\text{wall}})) H(u - e\phi_{\text{wall}}), \quad (\text{B4})$$

$$I(u) = N(u + u_i) \sigma_i(u + u_i) f(u + u_i) \quad (\text{B5a})$$

when neglecting secondary electrons from ionization, or

$$I(u) = 2N(2u + u_i) \sigma_i(2u + u_i) f(2u + u_i) \quad (\text{B5b})$$

when including ionization secondaries, and

$$S(u) = \delta(u) \int_{e\phi_{\text{wall}}}^{\infty} \frac{u'}{w} \gamma_s(u' - e\phi_{\text{wall}}) f(u') du'. \quad (\text{B6})$$

In this notation, Eq. (11) becomes

$$\begin{aligned} \frac{d}{du} \left[ D(u) \frac{df}{du} \right] + \frac{d}{du} [G(u) f] \\ - J(u) f(u) - W(u) f(u) = -I(u) - S(u). \end{aligned} \quad (\text{B7})$$

### Numerical Scheme

This equation is discretized on an equidistant grid of  $K$  points using 2<sup>nd</sup>-order accurate central differences and written as a matrix equation  $\mathbf{A} \mathbf{f} = \mathbf{b}$ . The boundary condition at infinite energy is expressed as  $f_K = 0$ . The maximum energy  $u_K$  must be large enough that the error in the boundary condition does not effect the solution at low energy. The normalization condition is expressed using Simpson's rule along the top row of  $\mathbf{A}$  and  $\mathbf{b}$ . The resultant matrix  $\mathbf{A}$  is tri-diagonal except for the first row and is easily inverted:

$$\begin{aligned} \left( \frac{1}{h^2} D_i - \frac{1}{4h^2} (D_{i+1} - D_{i-1}) - \frac{1}{2h} G_i \right) f_{i-1} \\ + \left( -\frac{2}{h^2} D_i - \frac{1}{2h} (G_{i+1} - G_{i-1}) - J_i - W_i \right) f_i \\ + \left( \frac{1}{h^2} D_i + \frac{1}{4h^2} (D_{i+1} - D_{i-1}) - \frac{1}{2h} G_i \right) f_{i+1} = -I_i - S_i. \end{aligned} \quad (\text{B8})$$

The ionization return term  $I$  is evaluated off the grid, so it appears on the right-hand-side of the matrix equation with the wall-secondary term  $S$ , which requires an integral of the EVDF. The wall-collision terms  $W$  and  $S$  also depend on the potential at the wall sheath. Therefore, the solution is an iterative procedure [24].

The iteration, shown schematically in Fig. B1, proceeds as follows: First, Eq. (B8) is solved with no inhomogeneous terms. From the first solution  $f^1$ , the wall potential is calculated from Eq. (14). The wall potential is chosen on the grid. The terms  $I$  and  $S$  are also calculated from the previous solution, using

cubic-spline interpolation to evaluate off-grid points. Equation (B8) is then solved including the inhomogeneous terms. This procedure is repeated until the relative error between two successive solutions is below  $10^{-5}$ , usually in 10-30 iterations.

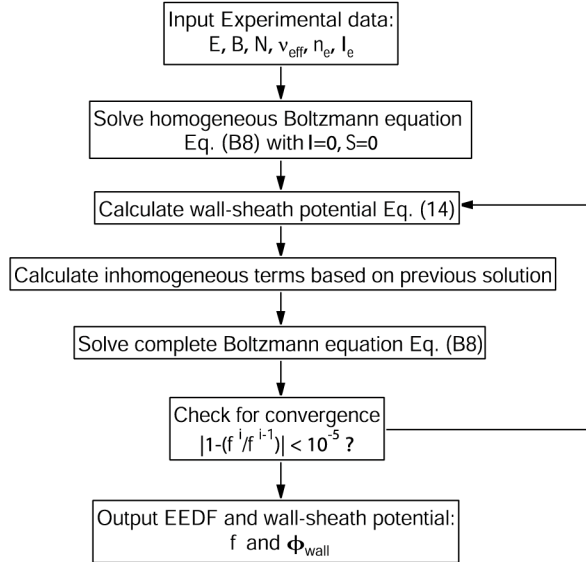


Figure B1-Flow chart of numerical solution

## References

- [1] G. S. Janes and R. S. Lowder, "Anomalous Electron Diffusion and Ion Acceleration in a Low-Density Plasma," *Phys Fluids* **9**, 1115 (1966).
- [2] A. I. Morozov and A. P. Shubin, "Electron kinetics in wall conductivity," *Sov. Tech. Phys. Lett.* **10**, 12-13 (1984)
- [3] A. I. Morozov and A. P. Shubin, "Electron kinetics in the wall-conductivity regime: I." *Sov. J. Plasma Phys.* **10**, 728-733 (1984)
- [4] A. I. Morozov and A. P. Shubin, "Electron kinetics in the wall-conductivity regime: II.," *Sov. J. Plasma Phys.* **10**, 734-735 (1984)
- [5] A. I. Bugrova, L. M. Volkova, V. A. Ermolenko, E. A. Kral'kin, A. M. Devyatov, and V. K. Kharchevnikov, "Dynamics of the Electron Energy Distribution Function in a Plasma Accelerator with Extended Acceleration Zone," *Teplofiz. Vys. Temp.* **19**, 1149 (1981) [Translated in *High Temp.* **19**, 822 (1982)].
- [6] A. I. Bugrova, A. I. Morozov, and V. K. Kharchevnikov, "Experimental investigation of near wall conductivity," *Fiz. Plazmy* **16**, 1469-1481 (1990) [Translated in *Sov. J. Plasma Phys.* **16**, 849-856 (1990)].
- [7] P. Degond, V. Latocha, L. Garrigues, and J. P. Boeuf, "Electron Transport in Stationary Plasma Thrusters," *Transp. Theory Stat. Phys.* **27**, 203-21 (1998).
- [8] V. Latocha, L. Garrigues, P. Degond, and J. P. Boeuf, "Numerical Simulation of Electron Transport in Stationary Plasma Thrusters, *in press*.
- [9] V. Yu. Fedotov, A.A. Ivanov, G. Guerrini, A. N. Vesselovzorov, and M. Bacal, "On the Electron Energy Distribution Function in a Hall-type Thruster," *Phys. Plasmas* **6**, 4360 (1999).
- [10] N. B. Meezan and M. A. Cappelli, "Electron Energy Distribution Function in a Hall Discharge Plasma," *AIAA Paper 2001-3326, 37<sup>th</sup> Joint Propulsion Conference*, Salt Lake City, UT, 2001.
- [11] N. P. Carleton and L. R. Megill, "Electron Energy Distribution in Slightly Ionized Air under the Influence of Electric and Magnetic Fields," *Phys. Rev.* **126**, 2089 (1962).
- [12] G. W. Sutton and A. Sherman, *Engineering Magnetohydrodynamics*, New York: McGraw-Hill, pp. 129-138 (1965).
- [13] E. Passoth, J. F. Behnke, C. Csambal, M. Tichy, P. Kudrna, Yu. B. Golubovskii, and I. A. Porokhova, "Radial Behaviour of the Electron Energy Distribution Function in the Cylindrical Magnetron Discharge in Argon," *J. Phys. D.: Appl. Phys.* **32**, 2655 (1999).
- [14] U. Kortshagen, C. Busch, and L. D. Tsengin, "On simplifying approaches to the solution of the Boltzmann equation in spatially inhomogeneous plasmas," *Plasma Sources Sci. Tech.* **5**, 1 (1996).
- [15] S. Yoshida, A. V. Phelps, and L. C. Pitchford, "Effect of Electrons Produced by Ionization on Calculated Electron-Energy Distributions," *Phys. Rev. A* **27**, 2858 (1983).
- [16] L. Jolivet and J. F. Roussel, "Effects of the secondary electron emission on the sheath phenomenon in a Hall thruster," *3<sup>rd</sup> International Conference on Spacecraft Propulsion (ESA/KNES)*, Cannes, France, 2000
- [17] E. Ahedo, P. Martinez-Cerezo, and M. Martinez-Sanchez, "Model of plasma-wall interaction effects in a Hall thruster," *AIAA Paper 2001-3323, 37<sup>th</sup> Joint Propulsion Conference*, Salt Lake City, UT, 2001.
- [18] N. B. Meezan, W. A. Hargus, Jr., and M. A. Cappelli, "Anomalous Electron Mobility in a Coaxial Hall Discharge," *Phys. Rev. E* **63**, 026410-1 (2001).
- [19] W. A. Hargus, Jr. and M. A. Cappelli, "Laser-induced fluorescence measurements of velocity within a Hall discharge," *Appl. Phys. B, Lasers Opt.* **B72**, 961-969

(2001).

- [20] N. B. Meezan and M. A. Cappelli, "Electron Density Measurements for Determining the Anomalous Electron Mobility in a Coaxial Hall Discharge Plasma," AIAA Paper 2000-3420, *36<sup>th</sup> Joint Propulsion Conference*, Huntsville, AL, 2000.
- [21] CPAT and Kinema Software, [www.csn.net/siglo](http://www.csn.net/siglo) (1998).
- [22] P. H. Dawson, "Secondary Electron Emission Yields of some Ceramics," *J. Appl. Phys.* **37**, 3644 (1966).
- [23] J. Fife and M. Martinez-Sanchez, "A Numerical Study of Low-Frequency Discharge Oscillations in Hall Thrusters," AIAA Paper 97-3052, *33<sup>rd</sup> Joint Propulsion Conference*, Seattle, WA, 1997.
- [24] D. Uhrlandt, M. Schmidt, and R. Winkler, "A Method to Solve the Nonlinear Kinetic Equation of the "Nonlocal Approach" Including Coulomb Interaction of Electrons," *Comp. Phys. Comm.* **118**, 185-199 (1999).